Partial hydrolysis of diphosphonate ester during the formation of hybrid TiO_2 nanoparticles : role of acid concentration

WILEY VCH

RESEARCH ARTICLE

Partial Hydrolysis of Diphosphonate Ester During the Formation of Hybrid TiO_2 Nanoparticles: Role of Acid Concentration

Bharadwaj Mysore Ramesha,[a] Bram Pawlak,[b] Daniel Arenas Esteban,[c] Gunter Reekmans,[b] Sara Bals,[c] Wouter Marchal,[b] Robert Carleer,[b] Peter Adriaensens,[b] and Vera Meynen*[a,d]

[a] B. Mysore Ramesha, Prof. Dr. V. Meynen
Laboratory of Adsorption and Catalysis (LADCA), Department of Chemistry
University of Antwerp
Universiteitsplein 1, 2610 Wilrijk, Belgium
Corresponding Author, E-mail: vera.meynen@uantwerpen.be

[b] B. Pawlak, Dr. G. Reekmans, Prof. Dr. W. Marchal, Prof. Dr. R. Carleer, Prof. Dr. P. Adriaensens
Analytical and Circular Chemistry (ACC), Institute for Materials Research (IMO-IMOMEC)
University of Hasselt
Agoralaan 1, 3590 Diepenbeek, Belgium

[c] Dr. D. Arenas Esteban, Prof. Dr. S. Bals
Electron Microscopy for Materials Research (EMAT) and NANOlab Centre of Excellence
University of Antwerp
Groenenborgerlaan 171, 2020 Antwerp, Belgium

[d] Prof. Dr. V. Meynen
Sustainable Materials Management
Flemish Institute for Technological Research (VITO NV)
Boeretang 200, 2400 Mol, Belgium

Supporting information for this article is given via a link at the end of the document.

Abstract: The hydrolysis of the phosphonate ester linker during the synthesis of hybrid (organic-inorganic) TiO_2 nanoparticles is important when forming porous hybrid organic-inorganic metal phosphonates. In the present work, a method was utilized to control the in-situ partial hydrolysis of the diphosphonate ester in presence of a titania precursor and in function of acid content and its impact on the hybrid nanoparticles was assessed. Organodiphosphonate esters, and more specific, their hydrolysis degree during the formation of hybrid organic-inorganic metal oxide nanoparticles, are relatively under explored as linkers. Here, a detailed analysis on the hydrolysis of tetraethyl propylene diphosphonate ester (TEPD) as diphosphonate linker to produce hybrid TiO_2 nanoparticles is discussed in function of acid content. Quantitative solution NMR spectroscopy revealed that during the synthesis of TiO_2 nanoparticles, an increase in acid concentration introduces a higher degree of partial hydrolysis of the TEPD linker into diverse acid/ester derivatives of TEPD. Increasing the HCl/Ti ratio from 1 to 3, resulted in an increase in degree of partial hydrolysis of the TEPD linker in solution from 4% to 18.8% under the here applied conditions. As a result of the difference in partial hydrolysis, the linker-TiO_2 bonding was altered. Upon subsequent drying of the colloidal TiO_2 solution, different textures, at nanoscale and macroscopic scale, were obtained dependent on the HCl/Ti ratio and thus the degree of hydrolysis of TEPD. Understanding such linker-TiO_2 nanoparticle surface dynamics is crucial for making hybrid organic-inorganic materials (i.e. (porous) metal phosphonates) employed in applications such as electronic/photonic devices, separation technology and heterogeneous catalysts.

Introduction

Titanium dioxide nanoparticles (TiO_2 NPs) are one of the ubiquitous materials used in a multitude of applications such as: catalyst supports,[1] photocatalysts,[2,3] sol-gel coatings[4] i.e. as protective coating on metallic implants,[5] electronic/photonic devices[6-8] and drug delivery systems.[9,10] They have therefore, been studied extensively with respect to their syntheses, properties and performances.[11-13] TiO_2 nanoparticles with tuneable structures are formed via the controlled assembly of molecular units in syntheses, such as (aqueous) sol-gel methods,[14] water-soluble titanium complexes,[15] and non-hydrolytic sol-gel routes.[16,17] In sol-gel methods, the hydrolysis and condensation of the precursor molecules are controlled in different ways to direct the growth of the titania clusters. The final nanoparticles properties are usually controlled by for example, altering the pH of the reaction medium,[18,19] the use of additives such as peptizing agents, ligands and/or surfactants[20,21] as well as the synthesis conditions.[22] Also, the choice of the mineral acids affects the properties TiO_2 nanoparticles in aqueous sol-gel methods.[23,24] However, the choice of acid, that might interact with the growing titanium oxo cluster, also influences the final morphology of the (porous) TiO_2.[25,26] Among titanium precursors, used to create TiO_2 nanoparticles, titanium alkoxides are a popular choice for solvent based synthesis. They are known to be highly reactive towards water and to the presence of other ingredients that direct their polymerization and influence the growth (rate) of the nanoparticles.[27,28] Thus, it is vital to understand the interplay of these ingredients in order to have precise control when it comes to the preparation of TiO_2 based

(hybrid) materials, in which material properties affect applications such as in electronic devices and catalysts.[29-31]

One of the ways to achieve control over the structure and properties of TiO_2 NPs, formed by bottom-up approaches in solution, is by the incorporation of surface-active ligands.[32,33] A wide variety of ligands have been employed for the creation of metal oxide nanoparticles such as: carboxylates, silanes and phosphonates.[34] Each of these different classes of ligands varies in the mode and strength of binding with the surface of the metal oxide clusters.[35,36] Silanes and phosphonate linkers have also been incorporated for the synthesis of porous hybrid inorganic-organic materials, where their addition in-situ during synthesis thus plays multiple roles of linking the organic group to the inorganic matrix while simultaneously affecting particle growth and interactions similar to the function of a ligand. Phosphonate-based linkers have stronger bonding towards metal oxides and offer stable phosphonate-metal oxide (P-O-M) linkages compared to organosilanes. However, they are not commonly used in metal oxide nanoparticle synthesis compared to the other types of ligands.[37-40] Nevertheless, the formation of stable hybrid organic-inorganic nanoparticles is important when considering e.g. sol-gel based or nanobuilding block approaches to produce controlled porous hybrid metal phosphonates. The phosphonate based linkers can be classified, based on their reactive groups, into two broad categories, i.e organophosphonic acids and organophosphonate esters. The choice between these two groups of linkers for the synthesis of metal oxides is mainly dependent on their reactivity towards metal oxide precursors (metal alkoxides or metal chlorides), solubility in solvents (polar/non-polar) and thermal stability. Among organophosphonate esters, the diphosphonate esters are interesting linkers that have been employed for metal oxide nanoparticles synthesis.[41] Nevertheless, employing diphosphonate esters as linkers, especially under acidic sol-gel conditions, producing a stable sol that can be used as a first step in the formation of porous hybrid organic-inorganic metal oxides (i.e. metal phosphonates), has not been well established. It has been shown by De Roo *et al.*[42] that the use of trioctylphosphine oxide (TOPO) as the ligand for metal oxide nanocrystal synthesis leads to a complex ligand binding modality on the surface of metal oxides, due to the degradation of TOPO under highly acidic conditions. Therefore, understanding the acid stability of the diphosphonate ester linker and its impact on the resulting material properties is essential for TiO_2 nanoparticle formation employing diphosphonate ester linker.

Insights in the hydrolysis of these diphosphonate esters under acid conditions are essential since they perform multiple roles in the synthesis of hybrid metal phosphonate nanoparticles (i) they are needed as a linker to connect the organic and inorganic parts of the hybrid material during synthesis, forming a hybrid structure with the organic groups covalently bonded and well distributed in the inorganic matrix. ii) While present during the synthesis of the inorganic matrix itself, they can also act as ligands to control the size and stability of the colloidal nanoparticles formed. Furthermore, the use of multifunctional (in casu difunctional) phosphonate precursors, provides the ability to link individual NPs into a network, forming porous hybrid organic-inorganic metal phosphonates when the nanoparticle solution is destabilized. Possible approaches to form controlled porous metal phosphonates starting from a stable nanoparticle solution are e.g. sol-gel based and/or nanobuilding block approaches. Nanobuilding blocks (NBBs) can be composed of uniform sized metal oxo clusters (<2 nm) or nanoparticles (2-100 nm) that are capped by organic linkers having two or more reactive functional groups able to link the nanoparticles in a structured way, forming porous tailored structures.[43,44] To prepare the metal oxo clusters NBBs, the highly reactive Ti(IV) precursors present a challenge due to the rapid rate of hydrolysis and condensation in the presence of certain organic ligands (for example, phosphonic acids with titanium alkoxides).[28,45] However, as the diphosphonate esters have lower reactivity towards titanium alkoxide precursors, we hypothesize that the properties of the hybrid nanoparticles could be controlled by partial hydrolysis.

Therefore, understanding the formation and the interfacial properties of these TiO_2 nanoparticles with attached and reactive diphosphonate linker groups is vital for the synthesis of hybrid organic-inorganic metal phosphonate. In the present work, a method was utilized to control the in-situ partial hydrolysis of the diphosphonate ester precursor in presence of the titania precursor and in function of acid content and its impact on the hybrid nanoparticles formed was assessed. An HCl containing ethanol solution in the presence of tetraethyl propylene diphosphonate ester (TEPD) was used as precursor for the diphosphonate linker (SI, Figure S1).[46] The amount of water added was maintained at a constant ratio of water/Ti = 15.6, which is more than the minimum amount of water required to hydrolyze the alkoxide groups of the titanium n-butoxide precursor and to avoid the influence of humidity. Therefore, the only variable component of the synthesis recipe was the amount of acid applied, represented by the HCl/Ti ratio of 1 – 3 (absolute concentration of HCl = 0.01 to 0.03 moles and a constant Ti concentration of 0.01 moles). Following the synthesis, a stable colloidal hybrid TiO_2 NPs dispersion could only be obtained when both HCl and TEPD were added (absence of only TEPD resulted in formation of white colloidal suspension with TiO_2 NPs and absence of HCl (in the presence of TEPD) resulted in gelation due to the rapid hydrolysis-condensation of titanium n-butoxide). The colloidal solution and the dried solid samples were characterized by solution NMR, PXRD, HAADF-STEM, Raman, TGA-DSC-MS, DLS, and solid-state NMR to reveal the impact of the acid concentration on the properties of the obtained hybrid TiO_2 NPs capped with (derivatives of) TEPD.

Results and Discussion

Powder X-ray diffraction (PXRD) patterns of the dried TiO_2 nanoparticles synthesized in the presence of TEPD linker under three HCl/Ti ratios show the presence of an anatase phase with considerable peak broadening (Figure 1). The crystallite sizes were estimated to be around ~5.0 nm as determined by the Scherrer equation calculated from the (101) and (200) reflections of anatase TiO_2. Apart from the anatase peaks, small peaks are found at $2\theta = 30°$, which might possibly be due to the (121) reflections of TiO_2 in brookite phase. Additionally, two small peaks

were found between 43-45°. The peak at 42.8° and 44° could belong to brookite and rutile phases respectively. To evaluate the effect of the addition of TEPD linker on the formation of TiO_2 nanoparticles, TEPD-free TiO_2 nanoparticles were prepared under similar conditions with the same HCl/Ti ratios. The powder XRD patterns of the TEPD-free TiO_2 NPs can be found in the SI, Figure S2. These TiO_2 nanoparticles also showed anatase phase with crystallite sizes around ~ 5.0 nm. The small peaks around 30° were also present in these TEPD-free TiO_2 NPs. The presence of traces of the brookite phase could be attributed to: (i) the consequence of employing aqueous synthesis methods which results in mixed phase TiO_2 and (ii) addition of HCl as acid in the synthesis of hybrid TiO_2 NPs leads to formation of anatase NPs with traces of brookite impurities.[16,18] It is rather difficult to estimate the percentage of brookite traces by PXRD due to the presence of sub < 5 nm crystallites.[47] However, the addition of the TEPD linker seems not to alter the growth of the TiO_2 NPs into a preferred crystalline phase.

Raman spectroscopy of the dried samples of TiO_2 NPs formed in the presence of TEPD linker was performed to observe the Ti-O vibrations and organophosphorus vibrations as shown in Figure 2. The peaks around 748 cm^{-1} correspond to the P-C vibrations of the propylene bridge and the peaks at 1034 cm^{-1} and 1190 cm^{-1} are from the P-O vibrations of the TEPD linker.[48,49] The intensity ratio of P-C/P-O vibrations becomes more prominent as the HCl/Ti ratio increases from 1 to 3 possibly due to the changes in the phosphorus environment that might be binding differently to the TiO_2 surface. The Ti-O vibrations of the TiO_2 NPs result in peaks at 150 cm^{-1} (E_{g1}), 413 cm^{-1} (B_{1g}), 510 cm^{-1} (A_{1g}/B_{1g}), and 640 cm^{-1} (E_{g1}) confirming the presence of anatase phase TiO_2. It is noticed that as the HCl/Ti ratio increases from 1 to 3, a shoulder at ~250 cm^{-1} becomes prominent. This peak can be attributed to the A_{1g} mode of the Ti-O vibrations in brookite, but no other peaks can be identified for the brookite phase. The TEPD-free TiO_2 NPs were also analyzed by Raman spectroscopy, which shows the anatase phase with blue-shifted E_{g1} peak and peak broadening (SI, Figure S3). However, the shoulder at ~250 cm^{-1} is not present in any of these samples. The blue shift (~144 cm^{-1} for bulk anatase) and broadening of the E_{g1} peak at 150 cm^{-1} in both TEPD and TEPD-free TiO_2 NPs might be attributed to phonon confinement effect in small nanocrystals <5 nm.[11,50,51,52] When the polymorphs of TiO_2 NPs are present in trace amounts with anatase as the majority phase, Raman spectra can only detect brookite when present in excess of 15%.[53] Therefore, Raman and PXRD results indicate the presence of mainly anatase TiO_2 with possible traces of brookite phase present.

The nanoscale morphology of dried samples of TiO_2 NPs synthesized in the presence of TEPD (derivatives) was

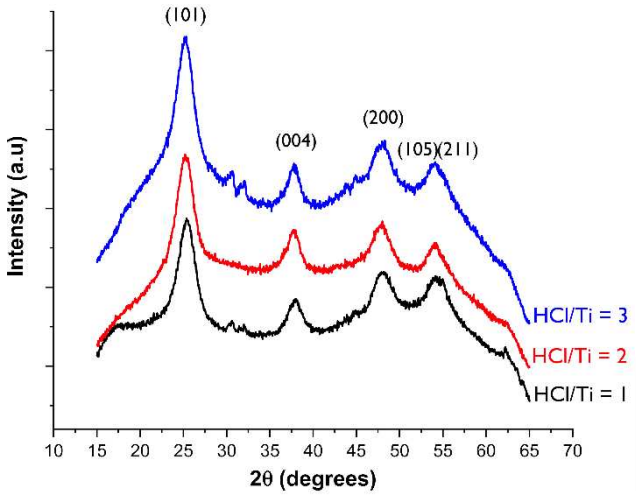

Figure 1. PXRD pattern for the TiO_2 NPs capped with TEPD linker.

investigated by high angle annular dark-field scanning transmission electron microscopy (HAADF-STEM) as illustrated in Figure 3. The TiO_2 NPs with TEPD were found to organize into fiber-like structures in the case of HCl/Ti = 1, which gradually changing morphology towards HCl/Ti = 3 as observed in the low magnification HAADF-STEM images (Figure 3A-C). The individual TiO_2 nanoparticles were found to mainly correspond to the anatase phase, as evidenced by high resolution HAADF-STEM images and their respective Fourier Transformations (FT) (Figure 3D-F). The high resolution HAADF-STEM images furthermore show an assembly with fiber-like morphology composed of small TiO_2 NPs of sizes ~2-5 nm. Apart from the smaller NPs, there were small fraction of larger nanoparticles of sizes ~10-20 nm. These larger nanoparticles were either brookite or rutile in phase and were single crystal-like as confirmed by FT patterns (SI, Figure S4). It should be noted that TEM is a local technique and that these measurements should be complemented by PXRD and Raman spectra indicating that most of the TiO_2 NPs were composed of anatase phase with traces of brookite phases. In the absence of TEPD, TiO_2 NPs did not show any self-assembled structure, like those observed in Figure 3, but discrete small agglomerations of anatase phase nanoparticles (SI, Figure S5). Thus, in the presence of the TEPD linker, the individual nanoparticles seemed to be surface capped favoring their self-organization into bigger structures. Moreover, it seems that with increasing HCl/Ti ratio, the nature of the TEPD linker was altered, which is hypothesized to cause the change of morphology of the assembly of TiO_2 NPs.

To provide more insights on the impact of HCl concentration on the (surface) properties of TEPD containing TiO_2 NPs, the hydrodynamic diameters of the colloidal solution were measured. The intensity-weighted (Z-average) diameters were 51.4, 27.4 and 31.2 nm for the HCl/Ti = 1, 2 and 3 respectively (SI, Figure S6). In solution the TiO_2 NPs capped with diphosphonate linker might be forming larger assemblies than the individual nanoparticle. Moreover, the HCl/Ti = 1 sample clearly has a higher hydrodynamic diameter than those at elevated HCl content. One of the possible reasons for this could be the presence of

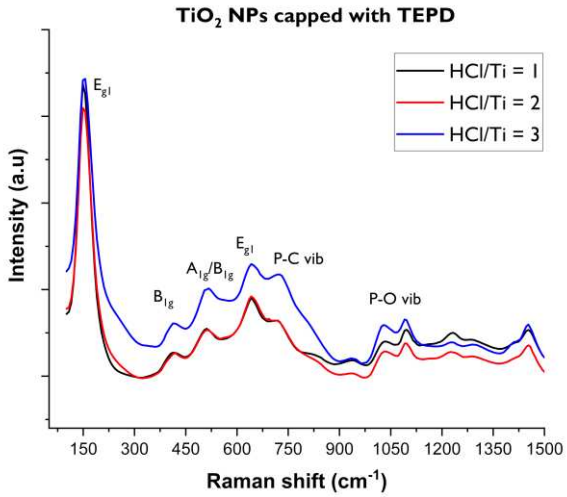

Figure 2. Raman spectra for the TiO_2 NPs capped with TEPD linker.

interparticle assembly of nanoparticles in solution at lower HCl amount.

To understand the TEPD linker binding to TiO_2 NPs better, the dried solid samples were studied by TGA/DSC under oxygen flow (Figure 4). Three weight loss regions could be identified from the thermograms: (i) first region, 130-340ºC due to loss of water/solvent and the initial decomposition of TEPD, (ii) the second region, 340-440ºC from the oxidation of the remaining TEPD linker that might be more strongly bonded to the TiO_2 surface, and (iii) high temperature weight loss >700ºC. The origin of the weight losses was determined by coupling a mass spectrometer to the TGA, which showed the release of CO, CO_2 and water in the 130-340ºC and 340-440ºC weight loss step. Whereas the weight loss at >700ºC takes place with only the release of CO_2 as seen by TG-MS (SI, Figure S7). Currently it is unclear why there is such as a large difference in the weight losses above 700ºC dependent on the HCl content. As there is no coinciding water release, it is expected to originate from a thermally formed carbonate phase(s). The weight losses in these three regions along with the total weight loss have been tabulated in SI, Table S1. It can be seen that the total weight losses were not equal across the three samples, although the samples were all prepared with the same initial amount of TEPD. The ICP-OES elemental analysis for the solid samples showed that Ti/2P atom ratios of 1.0, 1.0, and 0.9 for HCl/Ti = 1, 2 and 3 respectively (SI, Table S2). Hence, the enhanced weight loss in HCl/Ti = 1 was not originating from a larger amount of P present in the sample. Two possible explanations could be at its origin: (i) remnant solvent adsorbed or trapped at the surface of the nanoparticles which could coincide with the difference of texture of the dried particles and (ii) (partial) hydrolysis of TEPD with loss of ethanol. The latter might also provide a different bonding of TEPD to the TiO_2 NPs, which appears to be changing dependent on the HCl/Ti ratio. For HCl/Ti = 1, the decomposition of TEPD in the first region (130–340ºC) is highest and decreases as the HCl/Ti ratio increases from 1 to 3. Similarly, the decomposition of TEPD in the second region (340-440ºC) shows a reduction in weight loss as the HCl/Ti ratio increases. Therefore, it supports the hypothesis that the TEPD linker undergoes changes during the synthesis depending

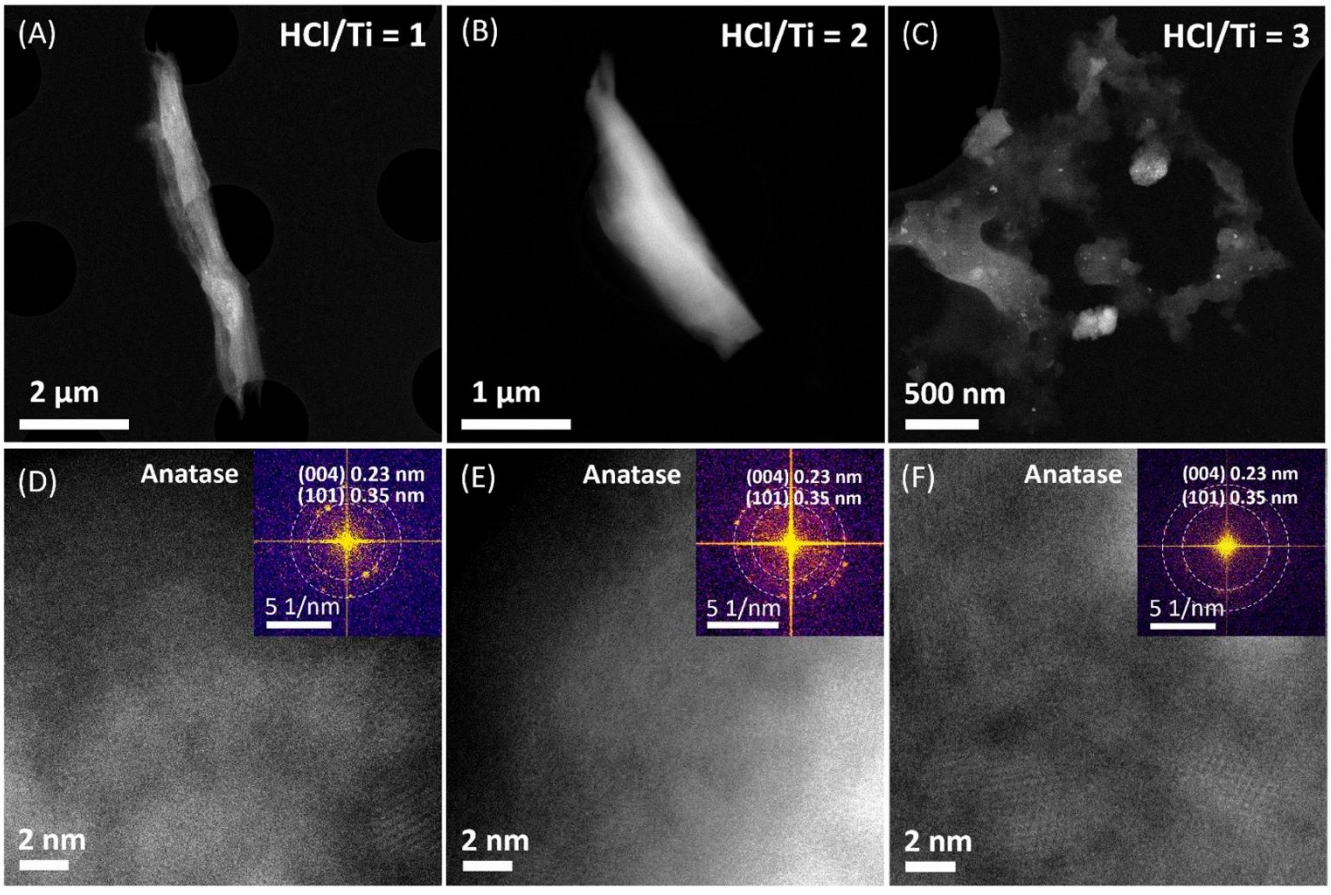

Figure 3. Low and high resolution HAADF-STEM images and their corresponding FT identifying the nanoparticles as anatase structure of TiO_2 NPs assembly capped with TEPD (derivatives) linker for HCl/Ti ratios of 1 (A, D), 2 (B, E) and 3 (C, F) respectively.

on the HCl/Ti ratio. Alternatively, one could hypothesize that the hydrolysis of the TEPD to its acid/ester form would be more extensive when the HCl/Ti ratio increases, leading to stronger bonding of the TEPD derivatives to TiO_2, which could reduce the evaporative oxidation weight loss. Also, the appearance of the weight loss above 700ºC seems to correlate to the enhanced HCl/Ti ratio, indicating a change in thermal stability of the linker. As only CO_2 was found in MS, it might be caused by carbonate formation due to higher temperature stability of the TEPD derivatives. However, no evidence of carbonate formation was found with variable temperature XRD in these materials (SI, Figure S8). It should be noted that the carbonate species might however be too small for detection or amorphous in nature.

A detailed investigation of the effect of the HCl/Ti ratio on the structure of the TEPD linker was accomplished by ^{1}H and ^{31}P NMR spectroscopy on the colloidal TiO_2 NPs solutions synthesized in the presence of TEPD. A stock solution was first prepared by dissolving TEPD, water, and benzophenone (as the internal standard for ^{1}H NMR) in ethanol. This stock solution was then refluxed at 90ºC in the presence of varying HCl amounts (0.01, 0.02 and 0.03 mol), and with or without titanium n-butoxide precursor, resulting in a colloidal TiO_2 NPs solution with TEPD and a blank TiO_2-free TEPD solution, respectively. In the synthesis recipe, the amounts of all ingredients were kept constant and only the HCl amount was varied.

The ^{31}P NMR spectra of the colloidal TiO_2 NPs solutions with TEPD and the TiO_2-free TEPD solutions with varying HCl/Ti ratios are presented in Figure 5a and 5b. Regarding the TiO_2-free TEPD solutions (Figure 5a), the solution without HCl shows a main resonance peak at 32.7 ppm, corresponding to the phosphorus environment in which the P-atom is bonded to $(OC_2H_5)_2$, =O, and -R (R = propylene bridge). Upon addition of varying HCl amounts, new peaks were observed downfield between 32.9-33.3 ppm and upfield between 28.5-30.7 ppm. These new resonance peaks increase in intensity as the HCl amount was increased. It is known that during reflux heating, alkyl phosphonate esters in the presence of acid (HCl or HBr) undergo hydrolysis to form alkyl phosphonic acids.[54] Based on similar studies focusing on partial hydrolysis of diphosphonate esters, these new resonance peaks can be attributed to partially hydrolyzed TEPD linker.[55,56]

The colloidal TiO_2 NPs solutions with TEPD display a similar main signal at 32.7 ppm, but less resonance peaks are observed, especially in the upfield region between 28.5-30.7 ppm (Figure 5b). Additional peaks are only observed around 32.9 ppm and 30 ppm and with reduced intensities (relative to the main peak at 32.7 ppm) as compared to the TiO_2-free TEPD solutions. Moreover, enlarged views of the ^{31}P spectra showed a gradual increase of broad signals with increasing amount of HCl. Such broad signals can only originate from TEPD species that are conformationally strongly immobilized, resulting in short T2 relaxation decay times

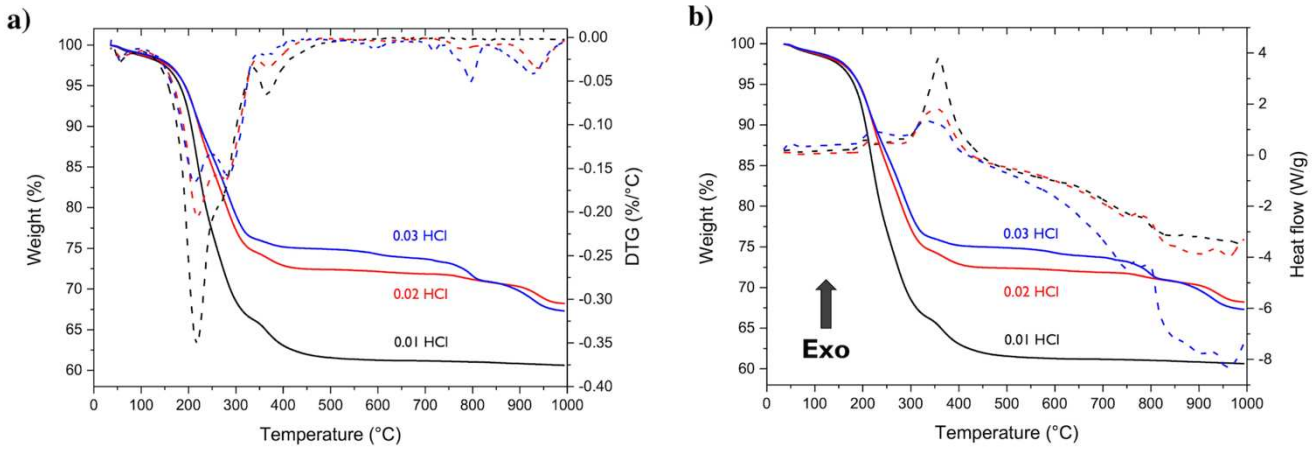

Figure 4. a) TGA-DTG and b) TGA-DSC of solid samples of TiO_2 NPs capped with TEPD (derivatives) linker measured under oxygen flow.

(SI, Figure S9). It can be suggested that these broad signals arise from (partially) hydrolyzed diphosphonate esters that were Ti-O-P coupled to the nanoparticle surface via Ti-O-P bonds (condensation between Ti-OH and hydrolyzed P-OH groups). This might explain the disappearance of some of the resonance peaks which were present in the ^{31}P-NMR spectra of the TiO_2-free TEPD solutions, as they become too broad to be observed without enlarging the spectra. The signals of (partially) hydrolyzed diphosphonate esters that were anchored at both P-sides (via condensation between Ti-OH groups and hydrolyzed P-OH groups) might become even so broad that they cannot be observed anymore. Based on these results, it can be concluded that the degree of partial hydrolysis of TEPD is dependent on the amount of HCl added, leading to the formation of partial ester/acid derivatives of TEPD that can be covalently attached to the TiO_2 surface via(multiple) Ti-O-P bonds.

To quantify the partial hydrolysis of TEPD, ^{1}H-NMR spectra were recorded for the TEPD solutions with and without TiO_2 NPs, all in the presence of benzophenone as internal standard (Figure 5c and d). In the ^{1}H spectra of TEPD dissolved in ethanol and heated in the absence of HCl (Figure 5c), resonance peaks are

found of methyl protons between 0.9-1.3 ppm from TEPD, ethanol and ethanol ^{13}C-satellite peaks. Next, the protons of the methylene units of the propylene bridge can be observed between 1.8-2 ppm. The resonance peaks between 3.25-3.8 ppm are from the methylene protons of ethanol. And finally, the -OCH_2- protons of TEPD are present as a complex signal between 4-4.15 ppm. The integration values of the proton signals of the propylene bridge (-CH_2-)$_3$ and the -OCH_2- of the ethoxy groups allow to calculate the degree of partial hydrolysis of the TEPD linker as function of HCl/Ti ratio. The normalized integration value of the methylene protons of the propylene bridge (1.8-2 ppm; normalized to the benzophenone internal standard) remained the same (~65; SI, Table 3) for the three samples and the sample without HCl. This indicates that the propylene bridge stayed intact without structural changes during the synthesis. Remark that a change in the signal shape is observed as the HCl amount increases due to changes in the ^{1}H-^{31}P heteronuclear J-coupling constants upon (partial) hydrolysis (SI, Figure S10). The integration value of the -OCH_2- signal of the ethoxy groups (4-4.15 ppm) on the other hand decreased as the HCl/Ti ratio increases due to the loss of ester groups by the partial hydrolysis of the TEPD. The degree of partial hydrolysis of TEPD could be determined from these changing integration values as 3.4%, 11.9% and 16.5% for HCl amounts of 0.01, 0.02 and 0.03 mol, respectively (relative to TEPD without HCl as illustrated in SI, Table S3).

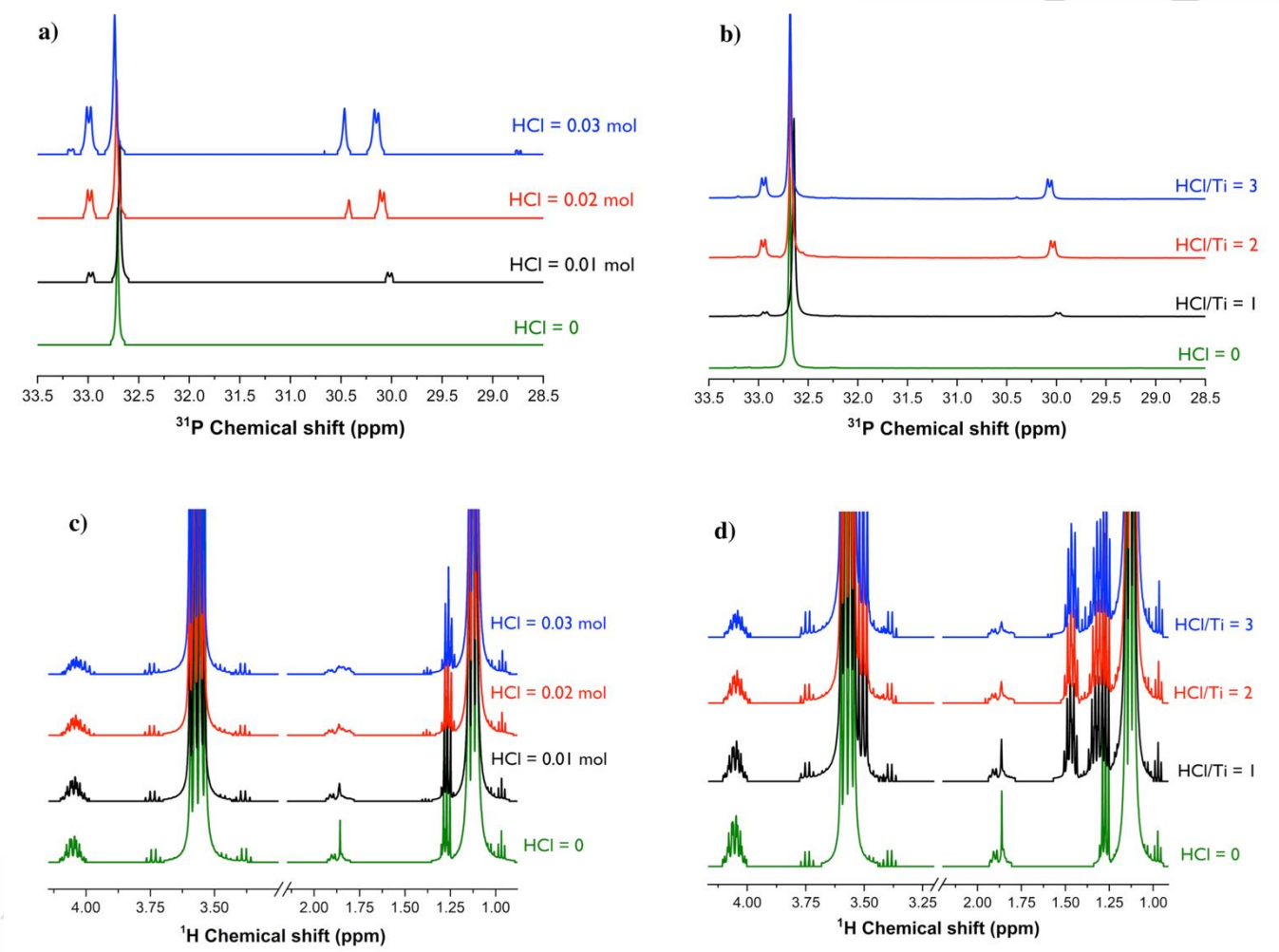

Figure 5. ^{31}P solution NMR spectra: (a) TiO_2-free TEPD solution and (b) colloidal solution of TEPD capped TiO_2 and ^{1}H solution NMR spectra: (c) TiO_2-free TEPD solution and (d) colloidal solution of TEPD capped TiO_2.

For the TEPD solutions with TiO_2 NPs (i.e. with titanium n-butoxide), the ^{1}H spectra are presented in Figure 5d. The spectra closely resemble the spectra of the TiO_2-free samples (Figure 5c) with additional resonances coming from n-butanol (around 1.10, 1.25, 1.50 and 3.55 ppm) released during the hydrolysis of titanium n-butoxide and formation of the TiO_2. To determine the degree of partial hydrolysis of TEPD in the presence of TiO_2 NPs, also the peak integration values of -$(CH_2)_3$- and -OCH_2- were used (Table 1). Similar to the TiO_2-free TEPD solution, the -OCH_2- integration value decreased as the HCl/Ti ratio increases due to the partial hydrolysis of TEPD. Interestingly, a gradual decrease of the integration value of the -$(CH_2)_3$- protons of the propylene bridge was observed as the HCl/Ti ratio goes from 1 to 3. This is in agreement with the appearance of broad signals in the ^{31}P-NMR spectra, which arise from (partially) hydrolyzed, immobilized diphosphonate esters that are coupled to the TiO_2 NPs via Ti-O-

P bonds. The signals of (partially) hydrolyzed diphosphonate esters that are anchored at both P-sides to the TiO_2 surface via Ti-O-P bonds probably become so broad that they even are not observed anymore, resulting in an underestimation of the integration values. In other words, assuming that there is no loss of TEPD from the synthesis mixture, it is suggested that a fraction of partially hydrolyzed TEPD was bonded so strongly to the TiO_2 NP surfaces that the conformational mobility was reduced to such an extent that the signals became too broad to be observed, explaining the decrease of the integration values of $-(CH_2)_3-$ bridge signals with HCl content. However, the percentage of strongly bonded TEPD could, for each HCl/Ti ratio, be calculated based on the difference in integration value for the $-(CH_2)_3-$ signal in the presence or absence of HCl. Based on this information, we were able to correct the (underestimated) integration values of the $-OCH_2-$ signal, and to determine the correct degree of partial hydrolysis of the TEPD in the presence of TiO_2 NPs. The resulting degrees of (partial) hydrolysis for HCl/Ti = 1, 2 and 3 were 4%, 10% and 18.8% respectively as shown in Table 1. The degree of partial hydrolysis calculated for both the TiO_2-free (SI, Table S3) and TiO_2-containing solutions are in good agreement. Therefore, it can be stated that the partial hydrolysis of the TEPD linker seems to be independent of the formation of the TiO_2 NPs network during the synthesis.

Regarding the texture of the solid materials after drying the TiO_2 NPs solutions, it was observed that it varied as a function of HCl/Ti ratio. While a gel-like texture was seen for HCl/Ti = 1, a rigid film that became powdery was obtained for HCl/Ti = 3. Materials with HCl/Ti = 2 possessed a texture in between these two extremes. The effect of the degree of partial hydrolysis of TEPD on the dried TiO_2 NPs samples was investigated by solid-state MAS and CP/MAS NMR for ^1H and ^{31}P nuclei. The ^1H MAS spectra reveal resonance peaks of the $-CH_3$ protons and $-CH_2$ protons of the $P-O-C_2H_5$ moiety around 1 ppm and 4 ppm respectively, while the $-(CH_2)_3-$ propylene bridge signals are situated around 1.7 ppm (Figure 6a). The resonance peaks broaden as the HCl/Ti ratio increases from 1 to 3, demonstrating that the diphosphonate moiety was indeed becoming more rigidly bonded to the TiO_2 NPs.

Sample ID	Integration ~4 ppm ($O-CH_2-$)	Integration ~1.8 ppm ($-P-(CH_2)_3-P-$)	Corrected integration ~4 ppm ($O-CH_2-$)	Hydrolysis (%)
HCl = 0	87.96	65.77	87.96	0.0
HCl/Ti = 1	77.55	60.41	84.43	4.0
HCl/Ti = 2	66.02	54.87	79.13	10.0
HCl/Ti = 3	58.57	53.92	71.44	18.8

Table 1. Peak integration values of the $O-CH_2$ and propylene $-(CH_2)_3-$ bridge signals obtained from the ^1H NMR spectra of colloidal TiO_2-NPs solutions synthesized in the presence of TEPD, for the calculation of the degree of partial hydrolysis of TEPD. Integration values were normalized towards benzophenone as internal standard.

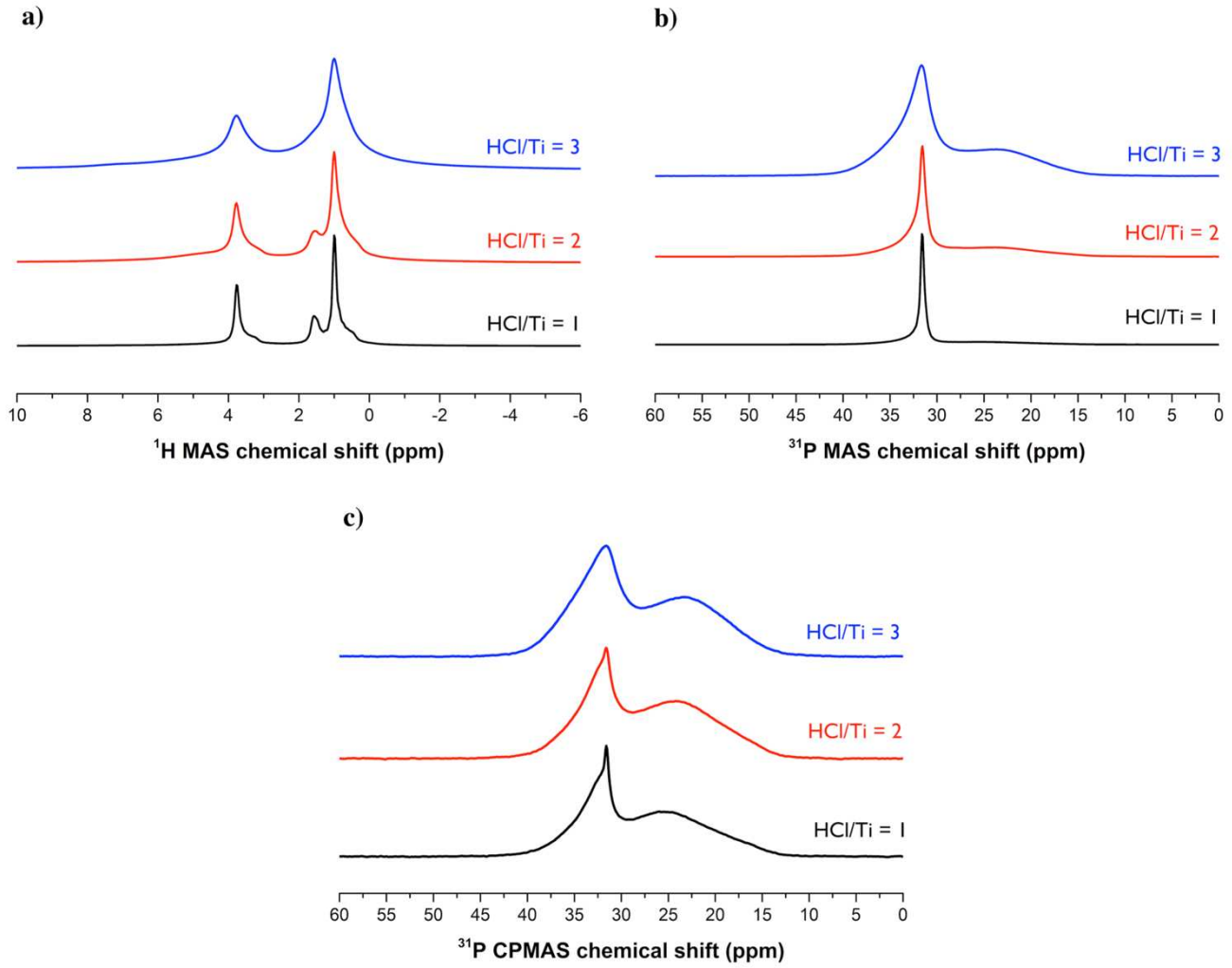

Figure 6. Solid-state NMR spectra: (a) ^{1}H MAS spectra, (b) ^{31}P MAS spectra and (c) ^{31}P CP-MAS spectra of the dried TiO_2 NPs with TEPD (derivatives) linker.

Similarly, the ^{31}P MAS spectra (Figure 6b) also show a gradual transition from a rather sharp peak around 32 ppm from mobile, little-hydrolyzed TEPD phosphonate ester for HCl/Ti = 1 (e.g., anchored with only one side of the diphosphonate moiety to the TiO_2 surface) to broader signals for HCl/Ti = 2 and 3 (Figure 6b). For HCl/Ti = 2, additional broad peaks of new phosphorus environments start to form around 24 and 35 ppm. These peaks became more prominent for HCl/Ti = 3. Please remark that MAS showed the rigid as well as the more mobile parts of the TEPD in the solid materials. To accentuate only the rigid part of the material, ^{31}P CP-MAS spectra were also recorded (strong dipolar interactions between ^{31}P and ^{1}H are needed for cross-polarization from the ^{1}H nuclei to ^{31}P nuclei). This clearly confirms the presence of new rigid phosphorus environments around 35 ppm and 24 ppm (Figure 6c). The broad signals were assigned to ^{31}P nuclei of partially hydrolyzed TEPD molecules that were immobilized by more P-O-Ti linkages to the TiO_2 surface. As a result of the partial TEPD hydrolysis and its further interaction with the titanium, different phosphorus environments appeared due to different binding modes of partially hydrolyzed TEPD phosphonate at the TiO_2 NP surface. This phenomenon has also been found in phosphonic acid modified TiO_2.[57,58]

To further evaluate the bonding nature of TEPD to the TiO_2 NPs, the HCl/Ti = 3 sample was exposed to a humid environment (100% relative humidity) in order to increase the mobility of especially the weakly bonded TEPD chains. Hereby, water will be in competition with the TiO_2 NPs surface for H-bonding, resulting in an increased flexibility of these TEPD chains. Upon exposure to humidity, the broad resonance peaks of the methyl (1 ppm) and methylene (4 ppm) protons in ^{1}H MAS spectrum and the 32 ppm signal in the ^{31}P MAS and CP-MAS spectra became narrower (SI, Figure S11). However, the ^{31}P CP-MAS resonance peak around 24 ppm did not change in bandwidth upon exposure to water. This confirms different bonding strengths to the TiO_2 NPs for the partially hydrolyzed phosphonate ester/acid. Whereas the phosphonate ester moiety interacts via weak hydrogen bonds (along with possibly van der Waals interactions) with the TiO_2 NPs, the partially hydrolyzed phosphonate ester/acid were more strongly bonded to TiO_2 NPs surface by one or more covalent Ti-O-P bonds.

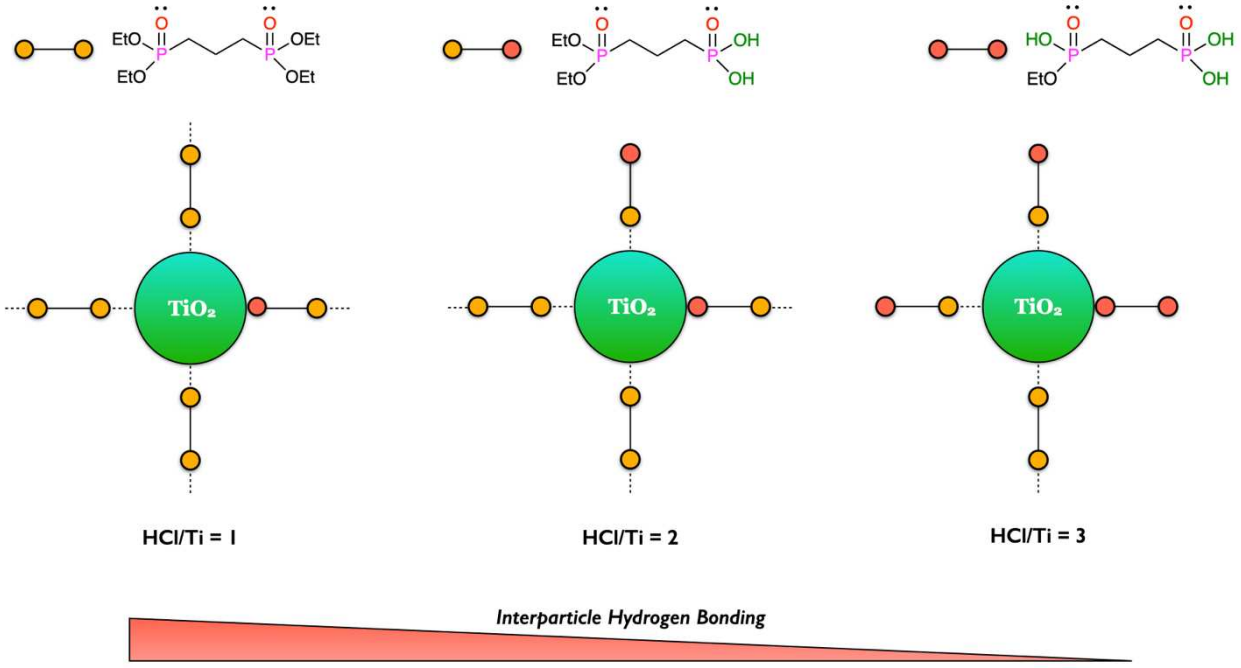

Scheme 1. Illustration of the formation of TEPD derivates upon partial hydrolysis under different HCl/Ti ratios in solution. The two types of surface bonding of TEPD (and derivatives) with the TiO_2 surface are shown (dotted lines for weak H-bonds and full lines for covalent bonds). Upon drying the less hydrolyzed TEPD can form inter-particle hydrogen bonding giving rise to gel-like texture, which gradually decreases as the partial hydrolysis increases with higher HCl amounts.

The TiO_2 NPs formed were mainly in anatase phase, since the water/Ti ratio and HCl/Ti ratio employed in the synthesis was meant to preferentially produce anatase phase.[43] However, a trace amount of brookite phase might be present because aqueous synthesis recipes often lead to the formation of TiO_2 with mixed phases.[59] The addition of TEPD to the synthesis, mainly seems to influence the organization of the TiO_2 NPs through surface stabilization. During the synthesis of the TiO_2 NPs, the TEPD linker undergoes partial hydrolysis leading to the formation of mixed phosphonate ester/acid species. The degree of partial hydrolysis of TEPD was dependent only on the HCl concentration. At low HCl/Ti ratio, the nanoparticles seem surface capped mainly by TEPD bearing phosphonate ester groups (almost unmodified TEPD) that arranges in a fiber-like morphology arising from intermolecular interactions between TEPD-capped TiO_2 NPs as illustrated schematically in Scheme 1. As the HCl/Ti ratio increases, more hydrolysis of the TEPD ester groups takes place, resulting in the formation of ester/acid phosphonate derivatives of TEPD that allow stronger bonding and reduced mobility of the diphosphonate linker. This leads to changing interactions and condensation reactions between diphosphonate moiety and the TiO_2 surface, inducing morphological changes from gel to a rigid texture.

Conclusion

In this work, the role of the HCl concentration on the fate of the diphosphonate linker TEPD and its impact on the final texture of the hybrid organic-inorganic TiO_2 nanoparticles have been described in detail. The sol method leads to the formation of colloidal anatase TiO_2 nanoparticles that have been capped by partially hydrolyzed TEPD linker. As the amount of HCl/Ti increased, the hydrolysis degree of TEPD enhanced and the extent of partial hydrolysis was quantitatively determined by ^1H NMR spectra. The degree of hydrolysis varied from ~4% for HCl/Ti = 1 to around ~18.8% for HCl/Ti = 3. Controlled drying of the colloidal solution led to textures that varied at nanoscale in forming different self-assembled fiber structures and at macroscale provided a gel-like to a rigid film for HCl/Ti = 1 to 3, respectively. The partial acid/ester derivatives of TEPD bonded to the TiO_2 surface in two types of binding: weaker bonded phosphonate ester moieties and stronger, more hydrolyzed moieties, covalently bonded to the TiO_2 nanoparticle surface, as evidenced by solid-state ^1H and ^{31}P MAS and CP-MAS NMR at elevated humidity. These results highlight the changes in morphology at nanoscale and macroscale, influenced by the hydrolysis degree of the diphosphonate ester linker that were *in-situ* hydrolyzed in an acidic synthesis. In this study, the impact of partial hydrolysis of the diphosphonate linker TEPD and its bonding to TiO_2 nanoparticle surface is observed, which is due to the differences in the mobility of the bonded linker, which affects the assembly of the nanoparticles. The incorporation of TEPD derivatives leads to the formation of stable colloidal TiO_2 NPs solution, with the partially hydrolyzed TEPD moieties strongly bonded to TiO_2 NPs surface depending on the HCl concentration. The degree of partial hydrolysis could be tailored to create TiO_2 nanobuilding blocks capped TEPD linkers, which is deemed important to create controlled, porous hybrid organic-inorganic

metal phosphonate networks by interconnecting the nanoparticles in a controlled structure in a second step. The latter was outside the scope of this study. These results are relevant for alkyl diphosphonate ester linkers as they undergo hydrolysis similar to TEPD (in the presence of HCl or HBr) and could be employed as starting precursor (nanoparticle) solutions for the creation of porous hybrid inorganic-organic metal phosphonates.

Experimental Section

Materials and Methods

Chemicals

Titanium (IV) n-butoxide (≥98% Acros), Hydrogen chloride (37% Acros), Tetraethyl propylene diphosphonate ester (≥95% Sikemia), Benzophenone (99% Acros) and Ethanol (≥99.9% EMSURE® Merck) were used as received.

Synthesis of Hybrid TiO_2 Nanoparticles

To three empty 100 mL round bottom flasks, 35 mL of ethanol was added and to each of them, tetraethyl propylene diphosphonate (1.42 mL, 0.005 mol) was added. Afterwards, 3 different amounts of concentrated HCl (37%) were added: 0.875 mL (0.01 mol), 1.76 mL (0.02 mol) or 2.51 mL (0.03 mol) of acid. Finally, a volume of 2.26 mL, 1.76 mL and 1.23 mL of DI water was added to the flasks containing 0.01 mol, 0.02 mol and 0.03 mol HCl, respectively. Therefore, the total amount of water in all three flasks was kept constant at 2.81 mL (0.156 mol). The solutions in the round bottom flasks were homogenized by stirring at ~400-500 rpm for a period of 15 minutes. Then, titanium (IV) n-butoxide (3.42 mL, 0.01 mol) was added during stirring, resulting in a clear, transparent solution. The solution was stirred (~400-500 rpm) for another 15 minutes at room temperature under ambient air. Then, the reaction mixtures were put under reflux at 90°C for 24 hours while stirring at 300 rpm. When the solution was cooled down to room temperature, a stable transparent colloidal solution was obtained. This colloidal solution was later transferred to a petridish and dried in an oven and maintained at 60°C for seven days. The texture of the final materials was different depending on the acid content, from gel-like (HCl/Ti=1; absolute HCl concentration of 0.01 mol) to a rigid transparent film (HCl/Ti=3; absolute HCl concentration of 0.01 mol). The rigid sample (HCl/Ti = 3) was grinded as a powder before characterizations (PXRD, Raman, TGA/TG-MS, Solid-state NMR, and HRTEM). The gel-like film was peeled from the petridish prior to characterization.

Preparation of Standard Solutions for NMR Analysis

For quantitative analysis of partial hydrolysis by ^{1}H NMR spectroscopy: in a 250 mL volumetric flask 6.20 g of benzophenone, as the internal standard, was dissolved in ethanol in the presence of 9.20 mL of TEPD (molar ratio of benzophenone/TEPD = 1). Then, from this stock solution, two batches of syntheses were performed: (i) TEPD solution without TiO_2, wherein 30 mL of the stock solution was transferred to four round bottom flasks, and to these four flasks, 0 mL (0 mol), 0.875 mL (0.01 mol), 1.76 mL (0.02 mol) and 2.51 mL (0.03 mol) of HCl (37%) was added. Finally, 2.81 mL, 2.26 mL, 1.76 mL and 1.23 mL of DI water was added to the flasks containing 0 mol, 0.01 mol, 0.02 mol and 0.03 mol HCl. These solution mixtures were stirred for 15 minutes (~400-500 rpm) at room temperature under ambient air and later put under reflux at 90°C for 24 hours at 300 rpm. (ii) For the TEPD solution with TiO_2, three solutions with 0.01, 0.02 and 0.03 moles of HCl, and 2.26 mL, 1.76 mL and 1.23 mL of DI water were prepared as described above. To these solution mixtures titanium n-butoxide (3.42 mL, 0.01 mol) was finally added and put under reflux at 90°C for 24 hours at 300 rpm. After reflux, the solutions were cooled to room temperature and analyzed by ^{1}H and ^{31}P NMR solution spectroscopy.

Characterization

Powder X-ray diffraction (PXRD) and variable temperature XRD for the TiO_2 NPs in the presence of TEPD was carried out on a Bruker D8 Discover XRD system with a Cu X-ray source (λ = 0.15406 nm) and a linear X-ray one -dimensional detector (Vantec) in the 2θ range from 15° to 65°. For the variable temperature XRD the samples were put on a sample heating stage inside a closed annealing chamber. The XRD measurements were carried out under oxygen atmosphere with a continuous flow rate of 500 sccm at atmospheric pressure. Samples were heated at a heating rate of 10°C/min to a maximum of 980°C. The temperature was measured by a K-type thermocouple. Every 8 seconds an XRD snapshot from 20-40° in 2θ was taken. In-situ scans were then plotted as a colour map with the temperature in the X-axis the 2θ in the Y-axis and the color as the XRD intensity with red being more intense diffraction peaks. For the TiO_2 NPs without TEPD linker PXRD was performed on a different diffractometer using a Bruker D8 Advance Eco equipped with Cu Kα radiation (λ = 0.15406 nm). Measurements were done in the 2θ range from 10° to 80° using a scanning speed of 0.04°/s in continuous mode. No further data treatment in terms of background removal was performed, the as recorded diffraction patterns have been presented as it is.

Raman spectra were recorded using a Micro-Raman spectroscopy from Horiba (Xplora Plus Microscope) equipped with a green 532 nm laser in the range 100 cm^{-1} to 3500 cm^{-1}. The spectra were recorded with following parameters: Acquisition time – 10s, Accumulation – 6, Real time display (RTD) time – 1, Grating – 650 (750 nm), Slit – 100 µm. No further data treatment in terms of background removal was performed, the as-recorded spectra have been presented as it is. The broad peak between 100 – 700 cm^{-1} are due to background scattering from glass slide (transparent samples).

DLS experiments for the colloidal solutions were performed on a Malvern zetasizer nanoseries (Malvern Panalytical, Malvern, UK) device using a 532 nm wavelength.

Thermogravimetric analyses (TGA) were recorded on a Mettler Toledo TGA-DSC 3+. The samples were measured in a continuous flow of oxygen (80 mL/min), heated from 30-1000°C with a heating ramp of 10°C/min.

TGA-MS were recorded by coupling the Mettler Toledo TGA-DSC 3+ with a Hiden HPR-20 mass spectrometer using same conditions for the TGA measurements. The samples were heated from 30-1000°C with a heating ramp of 10°C/min in a continuous flow of oxygen at 80 mL/min. The MS was setup to screen for m/z values from 2-100. A Faraday detector was set for m/z values of 31-41 and a SEM detector was used for m/z values of 2-30 and 42-100.

Inductively Coupled Plasma Optical Emission Spectroscopy (ICP-OES), Agilent Technologies 5100 ICP-OES was performed to determine the Ti and P content of the samples. The samples were digested in a solution of 1.5 mL HNO_3 (67–69%), 1.5 mL HF (48%) and 3 mL H_2SO_4 (96%) for 24 h at 250 °C. After digestion, 16 mL of H_3BO_3 (4%) was added to neutralize the HF.

High angle annular dark-field scanning transmission electron microscopy (HAADF-STEM) images and selected area electron diffraction were acquired on an aberration-corrected Titan Thermo Fischer QU-Ant-EU electron microscope operating at 300 keV.

^{1}H and ^{31}P liquid-state NMR – The ^{1}H-NMR spectra were measured at room temperature on a 400 MHz Varian Inova spectrometer equipped with a 5 mm OneNMR PFG probe head. No deuterated solvent was added. The chemical shift (ppm) was calibrated to TMS (0 ppm). All spectra were acquired with a 45° pulse of 3.45 µs, a spectral width of 6.4 kHz, an acquisition time of 3 s, a relaxation delay of 15 s and 64 accumulations. A line broadening of 0.2 Hz was applied before Fourier transformations to the frequency domain.

The ^{31}P-NMR spectra were acquired on the same spectrometer using the same 5 mm probe. No deuterated solvent was added. The chemical shift (ppm) was calibrated relatively to orthophosphoric acid at 0 ppm. Free induction decays were collected with a 75° pulse of 17 µs, a spectral width of 33.3 kHz, an acquisition time of 2.2 s, a relaxation delay of 10 s and 32 accumulations. A line broadening of 3 Hz was applied before Fourier transformation to the frequency domain.

High-resolution ^{1}H-MAS, ^{31}P-MAS and ^{31}P-CPMAS solid-state NMR – Solid-state ^{1}H-MAS spectra were acquired on a Jeol ECZ600R 600 MHz spectrometer equipped with a 3.2 mm wide VT Range HXMAS probe. Magic angle spinning was performed at 12 kHz. The chemical shift scale (ppm) was calibrated to TMS (0 ppm). Acquisition parameters used were: a spectral width of 100 kHz, a 80° pulse length of 2.0 µs, an acquisition time of 16.4 ms, a relaxation delay time of 15 s and 32 accumulations. A line-broadening of 20 Hz was applied before Fourier transformations to the frequency domain.

Solid-state ^{31}P-MAS spectra were acquired on the same spectrometer with the same probe. Magic angle spinning was performed at 12 kHz. The signal of KH_2PO_4 was used to calibrate the phosphorus chemical shift scale (3.9 ppm). Acquisition parameters used were: a spectral width of 122 kHz, a 80° pulse length of 3.5 µs, an acquisition time of 13.4 ms, a relaxation delay of 30 s and 256 accumulations. High power proton dipolar decoupling during acquisition was set to 75 Hz. A line-broadening of 50 Hz was applied before Fourier transformation to the frequency domain.

Solid-state ^{31}P-CPMAS (Cross-Polarization Magic Angle Spinning) spectra were acquired on the same spectrometer with the same probe. Magic angle spinning was performed at 12 kHz. The signal of KH_2PO_4 was used to calibrate the phosphorus chemical shift scale (3.9 ppm). Acquisition parameters used were: a spectral width of 122 kHz, a 90° pulse length of 2.24 µs, an acquisition time of 13.4 ms, a relaxation delay of 5 s, a spin-lock field of 50 kHz, a contact time of 1.5 ms and 256 accumulations. High power proton dipolar decoupling during acquisition was set to 75 Hz. A line-broadening of 50 Hz was applied before Fourier transformation to the frequency domain.

Acknowledgements

This work was supported by the Research Foundation-Flanders (FWO Vlaanderen) Project G.0121.17N. The work was further supported by Hasselt University and the Research Foundation-Flanders (FWO Vlaanderen) via the Hercules project AUHL/15/2 – GOH3816N. V.M. acknowledges the Research Foundation—Flanders (FWO) for project K801621N. B.M R acknowledges, Prof. Dr. Christophe Detavernier and Dr. Davy Deduystche (COCOON, Ghent University) for PXRD and VT-XRD measurements, Prof. Dr. Christophe Van De Velde (iPRACS, University of Antwerp) and Dr. Radu Ciocarlan (LADCA, University of Antwerp) for helpful discussions on PXRD measurements and Dr. Nick Gys (University of Antwerp and VITO) for ICP-OES measurements.

Author Contributions

Bharadwaj Mysore Ramesha: Writing – Original Draft, Visualization, Validation, Methodology, Investigation, Formal analysis, Data curation, Conceptualization.

Bram Pawlak: Writing – Review & Editing, Methodology, Conceptualization.

Daniel Arenas Esteban: Writing – Review & Editing, Formal analysis, Investigation.

Gunter Reekmans: Writing – Review & Editing, Methodology, Formal analysis, Investigation.

Sara Bals: Writing – Review & Editing, Investigation.

Wouter Marchal: Writing – Review & Editing, Supervision, Methodology, Conceptualization.

Robert Carleer: Writing – Review & Editing, Supervision, Methodology, Funding acquisition, Conceptualization.

Peter Adriaensens: Writing – Review & Editing, Supervision, Methodology, Funding acquisition, Conceptualization.

Vera Meynen: Writing – Review & Editing, Supervision, Methodology, Funding acquisition, Conceptualization.

The manuscript was written through contributions of all authors. All authors have given approval to the final version of the manuscript.

Conflict of Interest

There are no conflicts to declare.

Keywords: Organodiphosphonate esters • Partial hydrolysis • Hybrid TiO_2 nanoparticles • Linker-nanoparticle binding • NMR spectroscopy

References

[1] S. Bagheri, N. M. Julkapli, S. B. A. Hamid. *Sci. World J.* **2014**, 2014, 727496.
[2] M. Pelaez, M. T. Nolan, S. C. Pillai, M. K. Seery, P. Falaras, A. G. Kontos, P. S. M. Dunlop, J. W. J. Hamilton, J. A. Byrne, K. O'Shea, M. H. Entezari, D. G. Dionysiou. *Appl. Cat. B.* **2012**, 125, 331-349.
[3] F. Han, V. S. R. Kambala, M. Srinivasan, D. Rajarathnam, R. Naidu. *Appl. Cat. A.* **2009**, 359, 1-2, 25-40.
[4] R. A. Caruso, J. H. Schattka, A. Greiner. *Adv. Mat.* **2001**, 13, 20, 1577-1579.
[5] W. Xia, K. Grandfield, A. Hoess, A. Ballo, Y. Cao, H. Engqvist. *J. Biomed. Mater. Res. Part B Appl. Biomater.* **2012**, 100, 1, 82-93.
[6] W. Q. Wu, Feng, H. L.; Chen, H. Y.; Kuang, D. B.; Su, C. Y. Recent *J. Mater. Chem. A.* **2017**, 5, 12699-12717.
[7] A. Vyatskikh, R. C. Ng, B. Edwards, R. M. Briggs, J. R. Greer. *Nano Lett.* **2020**, 20, 3513-3520.
[8] J. Bai, B. Zhou. *Chem. Rev.* **2014**, 114, 19, 10131-10176.
[9] Z. F. Yin, L. Wu, H. G. Yang, Y. H. Su. *Phys. Chem. Chem. Phys.* **2013**, 15, 4844-4858.
[10] D. Ziental, B. Czaryczynska-Goslinka. *Nanomaterials.* **2020**, 10(2), 387.
[11] X. Chen, S. S. Mao. *Chem. Rev.* **2007**, 107, 7, 2891-2959.
[12] R. Zhang, A. A. Elzatahry, S. S. Al-Deyab, D. Zhao. *Nano Today.* **2012**, 7, 344-366.
[13] M. Cargnello, T. R. Gordon, C. B. Murray. *Chem. Rev.* **2014**, 114, 19, 9319-9345.
[14] D. P. Macwan, P. N. Dave, S. Chaturvedi. *J. Mater.Sci.* **2011**, 46, 3669-3686.
[15] Q. D. Truong, L. X. Dien, D. N. Vo, T. S. Le. *J. Solid State Chem.* **2017**, 251, 143-163.
[16] M. Niederberger. *Acc. Chem. Res.* **2007**, 40, 9, 793-800.
[17] M. Gopal, W. J. Moberly Chan, L. C. De Jonghe. *J. Mater. Sci.* **1997**, 32, 6001-6008.
[18] G. Li, K. A. Grey. *Chem. Mater.* **2007**, 19, 1143-1146.
[19] T. A. Kandiel, A. Feldhoff, L. Robben, R. Dillert, D. W. Bahnemann. *Chem. Mater.* **2010**, 22, 2050-2060.
[20] C. T. Dinh, T. D. Nguyen, F. Kleitz, T. O. Do. *ACS Nano.* **2009**, 3, 11, 3737-3743.
[21] P. Voepel, C. Seitz, J. M. Waack, S. Zahn, T. Leichtweiss, A. Zaichenko, D. Mollenhauer, M. Voggenreiter, S. Polarz, B. M. Smarsly. *Cryst. Growth Des.* **2017**, 17, 5586-5601.
[22] T. A. Kandiel, L. Robben, A. Alkaim, D. W. Bahnemann. *Photochem. Photobiol. Sci.* **2013**, 12, 602-609.
[23] S. L. Isley, R. L. Penn. *J. Phys. Chem. B.* **2006**, 110, 31, 15134-15139.
[24] S. L. Isley, R. L. Penn. *J. Phys. Chem. C.* **2008**, 112, 12, 4469-4474.
[25] S. Loreto, H. Vanrompay, M. Mertens, S. Bals, V. Meynen. *Eur. J. Inorg. Chem.* **2018**, 1, 62-65.
[26] S. Loreto, H. Vanrompay, M. Mertens, S. Bals, V. Meynen. *Eur. J. Inorg. Chem.* https://doi.org/10.1002/ejic.201801434.
[27] V. G. Kessler, G. I. Spijksma, G. A. Seisenbaeva, S. Hakansson, D. H. A. Blank, H. J. M. Bouwmeester. *J. Sol-Gel Sci. Techn.* **2006**, 40, 163-179.
[28] G. A. Seisenbaeva, V. G. Kessler. *Nanoscale.* **2014**, 6, 6229-6244.
[29] H. Liu, K. Cao, L. Jiao, Y. Wang, H. Yuan. *ACS Appl. Mater. Interfaces.* **2015**, 7, 21, 11239-11245.
[30] X. Wang, J. Q. Meng, M. Wang, Y. Xiao, R. Yiu, Y. Xia, Y. Yao, E. Metwalli, Q. Zhang, B. Qiu, Z. Liu, J. Pan, L. D. Sun, C. H. Yan, P. M. Buschbaum, Y. J. Cheng. *ACS Appl. Mat. Interfaces.* **2015**, 7, 43, 24247-24255.
[31] Q. Wu, F. Huang, M. Zhao, J. Xu, J. Zhou, Y. Wang. *Nano energy.* **2016**, 24, 63-71.
[32] J. Polleux, N. Pinna, M. Antonietti, M. Niederberger. *Adv. Mater.* **2004**, 16, 5, 436-439.
[33] J. Polleux, N. Pinna, M. Antonietti, C. Hess, U. Wild, R. Schlogl, M. Niederberger. *Chem. Eur. J.* **2005**, 11, 12, 3541-3551.
[34] S. Mallakpour, M. Madani. *Prog. Org. Coat.* **2015**, 86, 194-207.
[35] J. De Roo, K. De Keukeleere, Z. Hens, I. Van Driessche. *Dalton Trans.* **2016**, 45, 13277-13283.
[36] J. De Roo, I. Van Driessche, J. C. Martins, Z. Hens. *Nat. Mater.* **2016**, 15, 517-521.
[37] S. Pawsey, M. McCormick, S. De Paul, R. Graf, Y. S. Lee, L. Reven, H. W. Spiess. *J. Am. Chem. Soc.* **2003**, 125**,** 14, 4174-4184.
[38] S. A. Paniagua, A. J. Giordano, O. L. Smith, S. Barlow, H. Li, N. R. Armstrong, J. E. Pemberton, J. L. Bredas, D. Ginger, S. R. Marder. *Chem. Rev.* **2016**, 116, 12, 7117-58.
[39] J. De Roo, Z. Zhou, J. Wang, L. Deblock, A. J. Crosby, J. S. Owen, S. S. Nonnenmann. *Chem. Mater.* **2018**, 30, 21, 8034-8039.
[40] S. P. Pujari, L. Scheres, A. T. M. Marcelis, H. Zuilhof. *Angew. Chem. Int. Ed.* **2014**, 53, 25, 6322-6356.
[41] C. Queffelec, M. Petit, P. Janvier, D. A. Knight, B. Bujoli. *Chem. Rev.* **2012**, 112, 7, 3777-3807.
[42] K. De Keukeleere, S. Coucke, E. De Canck, P. V. D. Voort, F. Delpech, Y. Coppel, Z. Hens, I. Van Driessche, J. S. Owen, J. De Roo. *Chem. Mater.* **2017**, 29, 23, 10233-10242.
[43] C. Sanchez, G. J. de A. A. Soler-Illia, F. Ribot, T. Lalot, C. R. Mayer, V. Cabuil, *Chem. Mater.*, **2001**, 13, 3061-3083.
[44] G. J. de A. A. Soler-Illia, C. Sanchez, B. Lebeau, J. Patarin, *Chem. Rev.*, **2002**, 102, 4093-4138.
[45] B. Mysore Ramesha, V. Meynen, *Materials,* **2020**, 13, 5366.
[46] E. Beyers, P. Cool, E. F. Vansant. *J. Phys. Chem. B.* **2005**, 109, 20, 10081-10086.
[47] C. F. Holder, R. E. Schaak. *ACS Nano.* **2019**, 13, 7, 7359-7365.
[48] K. Moedritzer, R. R. Irani. *J. inorg. nucl.* **1961**, 22, 3-4, 297-304.
[49] L. van Haverbeke, H. O. Desseyn, M. A. Herman. *Bull. Soc. Chim. Belg.* **1972**, 81, 1, 547-554.
[50] V. Swamy, A. Kuznetsov, L. S. Dubrovinsky, R. A. Caruso, D. G. Shchukin, B. C. Muddle. *Phys. Rev. B.* **2005**, 71, 184302.
[51] Y. L. Du, Y. Deng, M. S. Zhang. *J. Phys. Chem. Solids.* **2006**, 67, 11, 2405-2408.
[52] G. Cappelletti, C. Ricci, S. Ardizonne, C. Parola, A. Anedda. *J. Phys. Chem. B.* **2005**, 109, 4458-4454.
[53] M. C. Ceballous-Chuc, C. M. Ramos-Castillo, J. J. Alvarado-Gil, G. Oskam, G. Rodriguez-Gattorno. *J. Phys. Chem. C.* **2018**, 122, 34, 19921-19930.
[54] C. M. Sevrain, M. Berchel, H. Couthon, P. A. Jaffres. *Beilstein J. Org. Chem.* **2017**, 13, 2186-2213.
[55] T. Kimura. *Angew. Chem. Int. Ed.* **2017**, 56, 43, 13459-13463.
[56] R. Wakabayashi, T. Kimura. *Chem. Eur. J.* **2019**, 25, 23, 5971-5977.
[57] D. Geldof, M. Tassi, R. Carleer, P. Adriaensens, A. Roevens, V. Meynen, F. Blockhuys. *Surf. Sci.* **2017**, 655, 31-38.
[58] N. Gys, L. Siemons, B. Pawlak, K. Wyns, K. Baert, T. Hauffman, P. Adriaensens, F. Blockhuys, B. Michielsen, S. Mullens, V. Meynen. *Appl. Surf. Sci.* **2021**, 566, 150625.
[59] M. Niederberger, M. H. Bartl, G. D. Stucky. *Chem. Mater.* **2002**, 14, 10, 4364-4370.

Entry for the Table of Contents

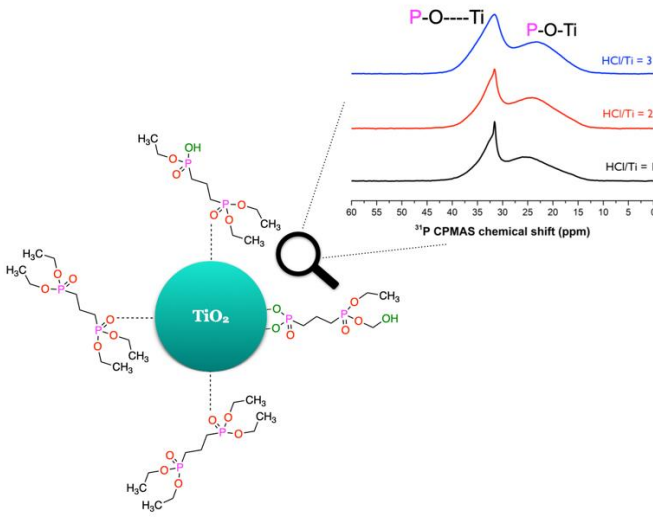

The extent of partial hydrolysis of tetraethyl propylene diphosphonate ester (TEPD) was altered by the acid content during the formation of hybrid organic-inorganic TiO_2 nanoparticles. Depending on the degree of partial hydrolysis, the TEPD (derivatives)-TiO_2 bonding in the obtained materials altered, as evidenced by solution and solid-state NMR.

Twitter

Bharadwaj Mysore Ramesha - @mrbharadwaj

Sara Bals - @EmatSarabals